SAND2017-1157J

Nanoscale Structure and Morphology of Sulfonated Polyphenylenes via Atomistic Simulations

Lauren J. Abbott and Amalie L. Frischknecht*

Sandia National Laboratories, Albuquerque, New Mexico 87185, United States

E-mail: alfrisc@sandia.gov

Abstract

We performed atomistic simulations on a series of sulfonated polyphenylenes systematically varying the degree of sulfonation and water content to determine their effect on the nanoscale structure, particularly for the hydrophilic domains formed by the ionic groups and water molecules. We found that the local structure around the ionic groups depended on the sulfonation and hydration levels, with the sulfonate groups and hydronium ions less strongly coupled at higher water contents. In addition, we characterized the morphology of the ionic domains employing two complementary clustering algorithms. At low sulfonation and hydration levels, clusters were more elongated in shape and poorly connected throughout the system. As the degree of sulfonation and water content were increased, the clusters became more spherical and a fully percolated ionic domain was formed. These structural details have important implications for ion transport.

For Table of Contents use only

Nanoscale Structure and Morphology of Sulfonated Polyphenylenes via Atomistic Simulations, Lauren J. Abbott and Amalie L. Frischknecht

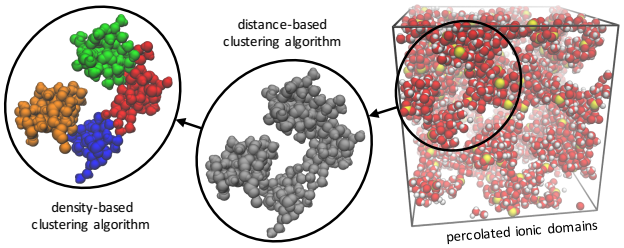

1 Introduction

Alternative energy devices like fuel cells, vanadium flow batteries, and lithium ion batteries employ polymer electrolyte membranes (PEMs) as an ion conducting separator between two electrodes.[1–3] To achieve the desired performance in these types of devices, PEMs generally should have high ionic conductivity, good mechanical properties, chemical and thermal durability, and dimensional stability. Perfluorosulfonic acid (PFSA) polymers, namely Nafion, represent the state of the art for PEMs. In these materials, the flexible backbone and side chains readily assemble into distinct hydrophilic and hydrophobic domains, which enable good ion conduction. However, PFSA polymers often suffer from high cost, reduced performance at low water contents and high temperatures, and long-term degradation. Recent research therefore has focused on a variety of alternative polymeric systems for PEMs.[4–8] Hydrocarbons incorporating aromatic groups in their backbones or side chains, such as polystyrene, poly(ether ether ketone), polysulfone, polyimide, and polyphenylene, have been explored extensively, because they have good mechanical properties over a broad temperature range. However, since the stiffer structures hinder phase separation to some extent, hydrocarbon PEMs often require higher degrees of sulfonation to improve ionic conductivities, which can lead to excessive swelling under hydrated conditions, negatively impacting the mechanical and dimensional stability of the membranes.

Fujimoto and coworkers have presented sulfonated Diels–Alder polyphenylene (SDAPP) as a promising alternative to Nafion for proton exchange membrane fuel cells[9,10] and electrolyte separators in vanadium redox flow batteries.[11,12] SDAPP has an aromatic backbone with six pendant phenyl groups per repeat unit, which provide up to six sites for post-sulfonation at the para positions, as shown in Figure 1. At lower sulfonation degrees (two or fewer sulfonic acid groups per monomer), SDAPP yields processable membranes that are thermally and mechanically robust. For example, the Young's moduli of SDAPP membranes in both the dry and hydrated states are an order of magnitude larger than that of Nafion.[9] Additionally, the unsulfonated polymer has a glass transition temperature of 388 °C, while

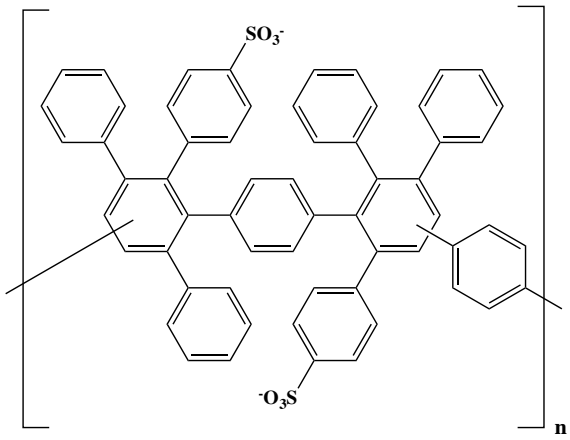

Figure 1: Chemical structure of SDAPP, shown with two sulfonic acid groups per monomer. Post-sulfonation occurs on the para position of the pendant phenyl groups, with a maximum of six possible sites of sulfonation.

the sulfonated versions thermally decompose below the glass transition temperature.[9] Although the SDAPP membranes have lower proton conductivities than Nafion at a similar ionic exchange capacity (IEC), they can achieve higher conductivities with a greater sulfonation level of two sulfonic acid groups per monomer.[9,10] Coupled with high conductivities, the SDAPP membranes also show lower methanol and vanadium crossover than Nafion.[10,11] Fujimoto and coworkers[10,12] have suggested that the stiffer structures of SDAPP hinder the ionic groups from fully phase separating, leading to narrower and more tortuous hydrophilic domains, but the nanoscale structure of these amorphous polymers is not understood fully.

The structural features of PEMs have a direct impact on their properties and performance. For example, water molecules become less associated with the polymer in larger hydrophilic domains, which increases proton diffusion, but also reduces the permselectivity.[13,14] The connectivity and tortuosity of the ionic domains are also important factors influencing the transport and mechanical properties. As such, researchers have suggested that an ideal morphology for PEMs includes continuous nano-sized hydrophilic domains or nanochannels.[3,5,14] In addition to the domain size and shape, the concentration and distribution of ionic groups are important, since there is a large energy barrier to proton transport between ionic sites with larger separations.[13] Although increasing the ionic concentration improves

the ionic conductivity by aiding in the formation of well connected channels, it can also have a negative impact on the mechanical properties and dimensional stability. These examples highlight the importance of understanding the structural features of PEMs, particularly in enabling the rational design of novel PEMs with enhanced performance. Unfortunately, common experimental techniques for characterizing the nanoscale structure of PEMs, including transmission electron microscopy (TEM), small-angle X-ray and neutron scattering (SAXS and SANS), and nuclear magnetic resonance (NMR), have notable limitations. Consequently, atomistic simulations can provide important insight into the atomic-level structure, as has been demonstrated for PFSA[15–19] and aromatic[20–23] PEMs.

In this work, we used atomistic simulations to study the structural properties of SDAPP (Figure 1) with a focus on the ionic domains. For computational efficiency, we assumed that the sulfonic acid groups were deprotonated in the simulations as sulfonate and hydronium ion pairs. As such, the simulations included proton transport only via the vehicular mechanism, which is dominatant over the Grotthuss mechanism at low humidity[3] and therefore should not have a significant impact on the structural properties examined here. We considered a total of 12 systems to systematically vary the sulfonation level given by the number of sulfonate groups per monomer (S = 1, 2, and 4), as well as the hydration level given by the number of water molecules per sulfonate group (λ = 3, 5, 10, and 20). The local structure and morphology of the ionic domains were dependent on the hydration and sulfonation levels, as these determine the strength of the ionic interactions. First, we examined the local structure around the ionic groups using radial distribution functions (RDFs) and coordination numbers. Then, we applied two different clustering algorithms to provide complementary insight into the ionic domain morphology. A distance-based method yielded a better descriptor of the cluster connectivity, while a density-based method yielded a better descriptor of local cluster size and shape.

2 Computational Methods

Initial structures of SDAPP oligomers were built via the Enhanced Monte Carlo (EMC) package.[24,25] Each periodic system contained 70 chains of three monomers each. We chose shorter oligomers here, since longer chains of these glassy polymers would have required prohibitively long simulation times to properly equilibrate. Three regio-isomeric repeat units with meta–meta, para–para, and meta–para configurations were chosen randomly based on experimentally measured compositions of 42, 40, and 18%, respectively, in similar systems.[26] After construction of the polymer backbones, we obtained systems with different sulfonation levels (S = 1, 2, and 4) by including a given number of sulfonate groups per repeat unit, the positions of which were chosen randomly from the six possible sites in the para positions of the pendant phenyl groups (Figure 1). These three sulfonation levels correspond to IECs of 1.19, 2.18, and 3.71 mequiv/g, respectively. We then achieved different hydration levels (λ = 3, 5, 10, and 20) by solvating the boxes with a given number of water molecules and hydronium ions randomly packed into the voids around the polymer chains. Each system had an equal number of hydronium ions and sulfonate groups to maintain a net charge of zero. For each of the 12 systems, we generated five boxes with random initial configurations following the process described above.

The bulky aromatic structures and strong electrostatics of SDAPP presented challenges for equilibration in the atomistic simulations, so we took care in choosing an adequate equilibration protocol. First, the box dimensions were gradually rescaled to a density of 0.7 g cm^{-3} during a 600 ps NVT MD simulation at 300 K. A 600 ps NVT MD simulation at 1000 K was then performed at this low density to allow the chain conformations to be sampled more freely, which helps to achieve system equilibration at all length scales.[27] We found that running a long NPT MD simulation at 1 atm was not adequate to bring the system to a realistic density due to the hindered dynamics of the glassy state. Instead, we adopted a procedure similar to that of Colina and coworkers,[28] where successive cycles of MD simulations are performed at high temperatures and pressures to help overcome large energy

barriers. Each cycle consisted of three MD runs: (i) a 50 ps NVT MD simulation at 1000 K, (ii) a 100 ps NVT MD simulation at 300 K, and (iii) a 50 ps NPT MD simulation at 300 K. A total of nine cycles were performed while progressively increasing the pressure of the NPT run to a high pressure, then decreasing back to 1 atm with the following pressure increments: 100, 1000, 10000, 5000, 1000, 500, 100, 10, and 1 atm. We chose pressure changes of no more than an order of magnitude during the decompression, which allowed the systems to respond smoothly and prevented significant levels of residual stress from forming.[27] The NPT MD simulation at 1 atm in the final cycle was extended to 2000 ps to allow the cubic simulation boxes to reach equilibrated dimensions of roughly 66 to 91 Å per side. The final densities of 1.08 to 1.27 g cm^{-3} are in agreement with experimental SDAPP densities of 1.1 to 1.2 g cm^{-3}.[11] Finally, each system underwent a thermal annealing cycle: (i) a 1000 ps NVT MD simulation at 2000 K, (ii) successive 100 ps NVT MD simulations at 1800, 1600, 1400, 1200, 1000, 900, 800, 700, 600, 500, and 400 K, and (iii) a final 1000 ps NVT MD simulation at 300 K. Following this equilibration protocol, long NVT MD production simulations were performed for 20 ns, during which frames were saved every 10 ps.

The polymer interactions were described using the OPLS-AA force field[29] with additional parameters for the sulfonate groups.[30,31] We also included improved parameters derived for biaryl structures,[32] which differentiate two aromatic carbons within the same aromatic ring from those in neighboring aromatic rings connected by a single bond (e.g., in biphenyl). In most cases, we applied the standard electrostatic charges from OPLS, except for benzene sulfonate groups.[33] Water was described using the rigid four-site TIP4P/2005 model[34] and hydronium ions with a flexible four-site model.[35] With the given parameters, the net charge of a hydronium ion ($+1\ e$) balances that of a sulfonate group ($-1\ e$). All MD simulations were performed in LAMMPS[36,37] using velocity-Verlet integration with a 1 fs timestep. Temperature and pressure were held constant in the NVT and NPT ensembles using a Nosé–Hoover thermostat and barostat with time constants of 0.1 ps. A short-range cutoff of 12 Å was used for nonbonded interactions, while long-range electrostatic interactions were imple-

mented using the PPPM technique with an accuracy of 3×10^{-5}. Water bonds and angles were constrained using the SHAKE algorithm.[38] We used VMD[39] for visualization of the molecular systems.

3 Results and Discussion

3.1 Local Structure

To examine the effect of the hydration and sulfonation levels on the local structure around the sulfonate groups, we compared partial RDFs for atoms within the ionic domains, specifically the sulfonate sulfurs (SO), hydronium oxygens (OWH), and water oxygens (OW). Given that the number of atoms can vary between these systems depending on the degree of sulfonation and water content, we renormalized the RDFs by the number density for a more direct comparison. First, RDFs for systems with a sulfonation level of $S = 1$ and varying hydration levels ($\lambda = 3$, 5, 10, and 20) are given in Figure 2 (a–c). The SO–OWH and SO–OW RDFs (Figure 2a and b) both have a large first peak around 4 Å and a smaller second peak around 6 Å, indicating the first and second solvation shells. The large first peaks in these cases resulted from the strong electrostatic interactions with the sulfonate groups, which were strongest with the oppositely charged hydronium ions. In the SO–OWH RDFs, the intensity of the first peak decreased at higher water contents, while the second peak intensity increased. Both peaks of the SO–OW RDFs increased in intensity. These results indicate that the sulfonate groups became more hydrated at higher water contents, which allowed more hydronium ions to move from the first to second solvation shell. In the SO–SO RDFs (Figure 2c), the first peak shifted to larger distances (4.85 to 6.45 Å) and decreased in intensity with greater water content, such that we observed no strong peak at a hydration level of $\lambda = 20$. The second peak in the SO–SO RDFs near 7.35 Å did not change in position significantly, but decreased slightly in intensity at the higher water contents. Thus, as the sulfonate groups became more hydrated, neighboring sulfonate groups were pushed further apart.

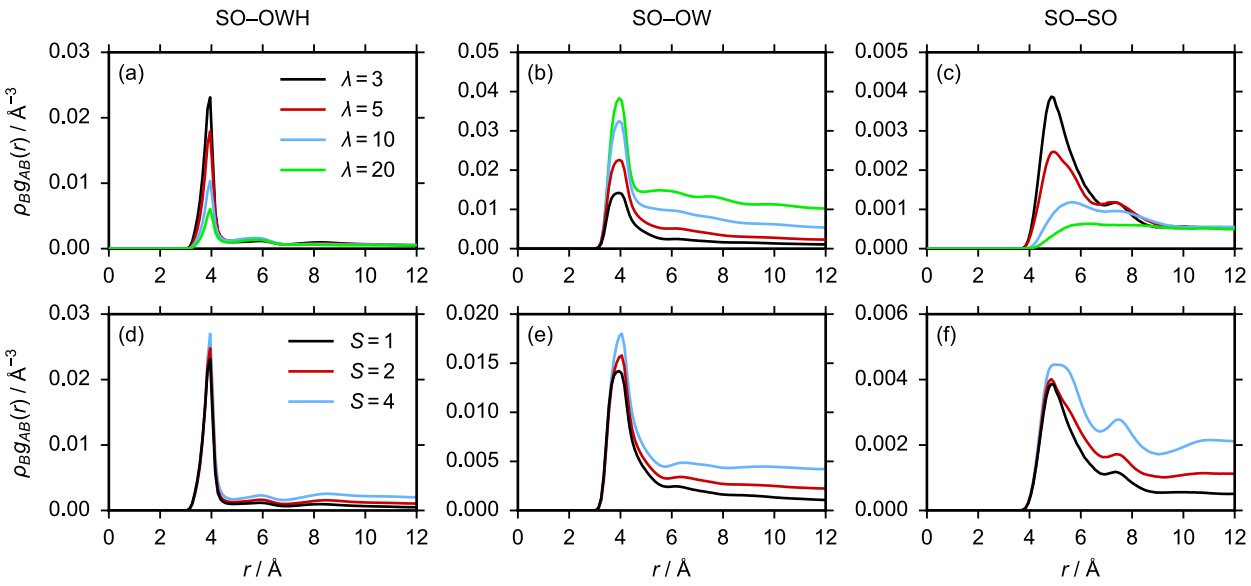

Figure 2: Partial radial distribution functions, $g_{\mathrm{AB}}(r)$, for sulfur–hydronium oxygen, SO–OWH, sulfur–water oxygen, SO–OW, and sulfur–sulfur, SO–SO, compared at (a–c) a sulfonation level of $S = 1$ and varying hydration levels, and (d–f) a hydration level of $\lambda = 3$ and varying sulfonation levels. The distributions were renormalized with the number density, ρ_B.

In Figure 2 (d–f), similar comparisons of RDFs are given for systems with a fixed hydration level of $\lambda = 3$ and varying sulfonation levels ($S = 1$, 2, and 4). The SO–OWH and SO–OW RDFs (Figure 2d and e) have two peaks around 4 and 6 Å resulting from the first and second solvation shells, as we noted for the varying hydration levels. In both cases, the peak intensities increased at higher degrees of sulfonation, but only slightly. This is due to the fact that the number of water molecules per sulfonate group remained constant at higher sulfonation levels, even though the total number of sulfonate groups and water molecules increased overall. In the SO–SO RDFs (Figure 2f), the positions of the first and second peaks located around 4.85 and 7.35 Å did not change significantly, indicating that neighboring sulfonate groups did not move further apart from each other, unlike what we observed for the variation in hydration levels. The intensities of both peaks increased at higher degrees of sulfonation due to the increased number density of sulfonate groups. Similar results have been reported for RDFs from simulations of other PFSA and aromatic PEMs. For instance, previous studies have shown sulfur–water oxygen and sulfur–hydronium oxygen RDFs that

had a large first peak around 4 Å and a second smaller peak near 6 Å.[15,16,18,22] Studies have also presented sulfur–sulfur RDFs with a first peak around 5 Å, which decreased in intensity and shifted to larger distances at higher water contents.[15–18] This suggests that a similar local structure exists around the ionic groups in a variety of sulfonated PEMs, despite the vastly different backbone structures.

Due to strong electrostatic interactions, hydronium ions are more tightly bound when coupled to several sulfonate groups and more liberated when surrounded by a greater number of water molecules. To quantify the local environment of the hydronium ions, we calculated the coordination numbers of sulfonate groups and water molecules, N_{SO} and N_{OW^*}, in the first solvation shell of the hydronium ions, where OW* includes either a water or hydronium oxygen atom. Here, cutoff distances were chosen to include the first peak in the corresponding RDFs. Two-dimensional histograms of N_{SO} versus N_{OW^*} are shown in Figure 3 for each system, where darker colors indicate regions explored more often during the simulations. The most populated local coordination states, as indicated by the darkest points in the plot, were generally consistent at all sulfonation levels, but varied with the water content. In particular, N_{OW^*} for the most probable state increased from 1 to 4 or 5 with increasing hydration, while N_{SO} decreased from 2 or 3 to 0. Notably, the proportion of time hydronium ions were neighbored by no sulfonate groups ($N_{\mathrm{SO}} = 0$) increased from 2% to around 46% with increasing water content, which indicates time during which the hydronium ions were not bound closely to any sulfonate groups. We also observed a large variation in the spread of data between the different systems. For example, the proportion of time hydronium ions spent in their most common state decreased significantly from 25% at a sulfonation level of $S = 1$ and hydration level of $\lambda = 3$ ($N_{\mathrm{OW}^*} = 1$ and $N_{\mathrm{SO}} = 2$) to only 11% at a sulfonation level of $S = 4$ and hydration level of $\lambda = 20$ ($N_{\mathrm{OW}^*} = 5$ and $N_{\mathrm{SO}} = 0$).

We have gained useful insight into the strength of interactions between the ionic groups by analyzing the local structure, which has important implications for ion transport. At low hydration levels of $\lambda = 3$ and 5, the ionic groups remained fairly close to one another,

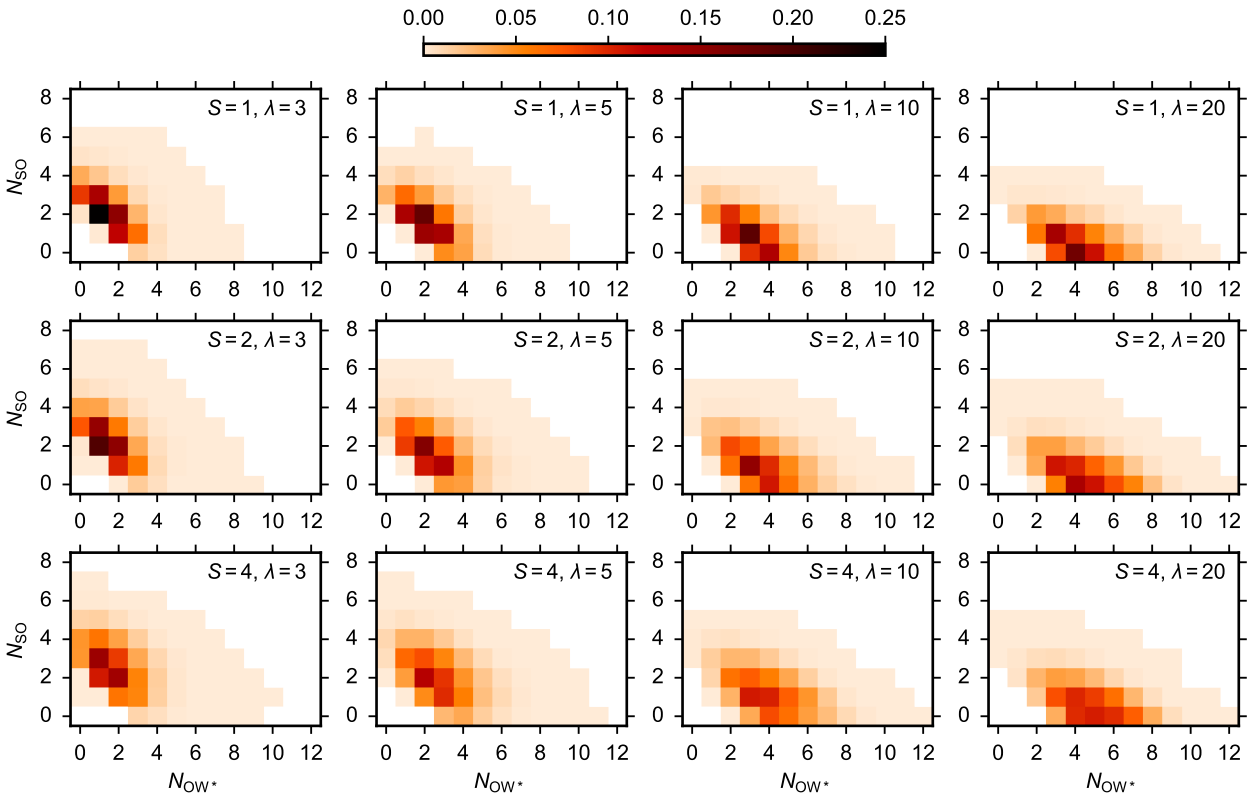

Figure 3: Two-dimensional histograms of the coordination numbers of sulfurs, N_{SO}, versus water and hydronium oxygens, N_{OW^*}, around hydronium oxygens for each system varying the sulfonation level (top to bottom) and hydration level (left to right). All systems use the same color map given above the plots, with darker colors indicating regions populated more frequently during the simulations.

with hydronium ions often bound closely to several sulfonate groups and neighbored by few water molecules. This would hinder ion transport, since hydronium ions are likely to remain stationary in this environment. At the higher hydration levels of $\lambda = 10$ and 20, however, both the sulfonate groups and hydronium ions became more hydrated. Moreover, we observed more solvent-separated ion pairs as the water content increased, as hydronium ions were able to move outside the first solvation shell of sulfonate groups. This observation is consistent with results from quantum calculations presented by Paddison and coworkers[40,41] in representative hydrated sulfonic acid systems, who found that ion pairs became separated after four to six water molecules were added. The increased proportion of time during which the hydronium ions were not bound closely to any sulfonate group at the higher hydration

levels suggests that the hydronium ions would be able to move more freely through the ionic domain, which would lead to improved ion transport.

3.2 Ionic Aggregates

In the simulations, we observed aggregation of the ionic groups and water molecules into nano-sized hydrophilic and hydrophobic domains. The atomic-level detail provided by the simulations enables important insight into the nanoscale structure of the ionic domains, including the shape, size, and connectivity, which is currently inaccessible to experimental techniques. Distance-based clustering algorithms have been used to this end in molecular simulation studies of ion-containing polymers,[15,17,23,42–44] where atoms were assigned to the same cluster if they were within a given cutoff distance from each other. In some situations, however, clusters defined in this way formed percolated networks that spanned the periodic boundaries, which limited the amount of information that could be obtained about the local nature of the cluster geometry, and hence restricted a meaningful comparison between systems. Therefore, we have adapted a density-based clustering algorithm[45] to provide an alternative definition of the clusters within the ionic domain, which we have applied to ionic aggregates in PEMs for the first time in this work. This algorithm isolates local regions of high density and can distinguish clusters that have some overlap. In Figure 4, snapshots of the hydrophilic domains for select systems varying both the sulfonation and hydration levels are compared for the distance-based and density-based algorithms, with each cluster shown in a different color. We found a significant difference in the two approaches. The distance-based algorithm identified one large extended cluster in many systems, providing information about the cluster connectivity. The density-based algorithm, on the other hand, defined an even distribution of distinct cluster in each case, which provided information about the cluster size and shape.

We employed the distance-based clustering algorithm with hydrogen atoms included in this work, as done by Bolintineanu et al.,[44] since the formation of hydrogen bond networks

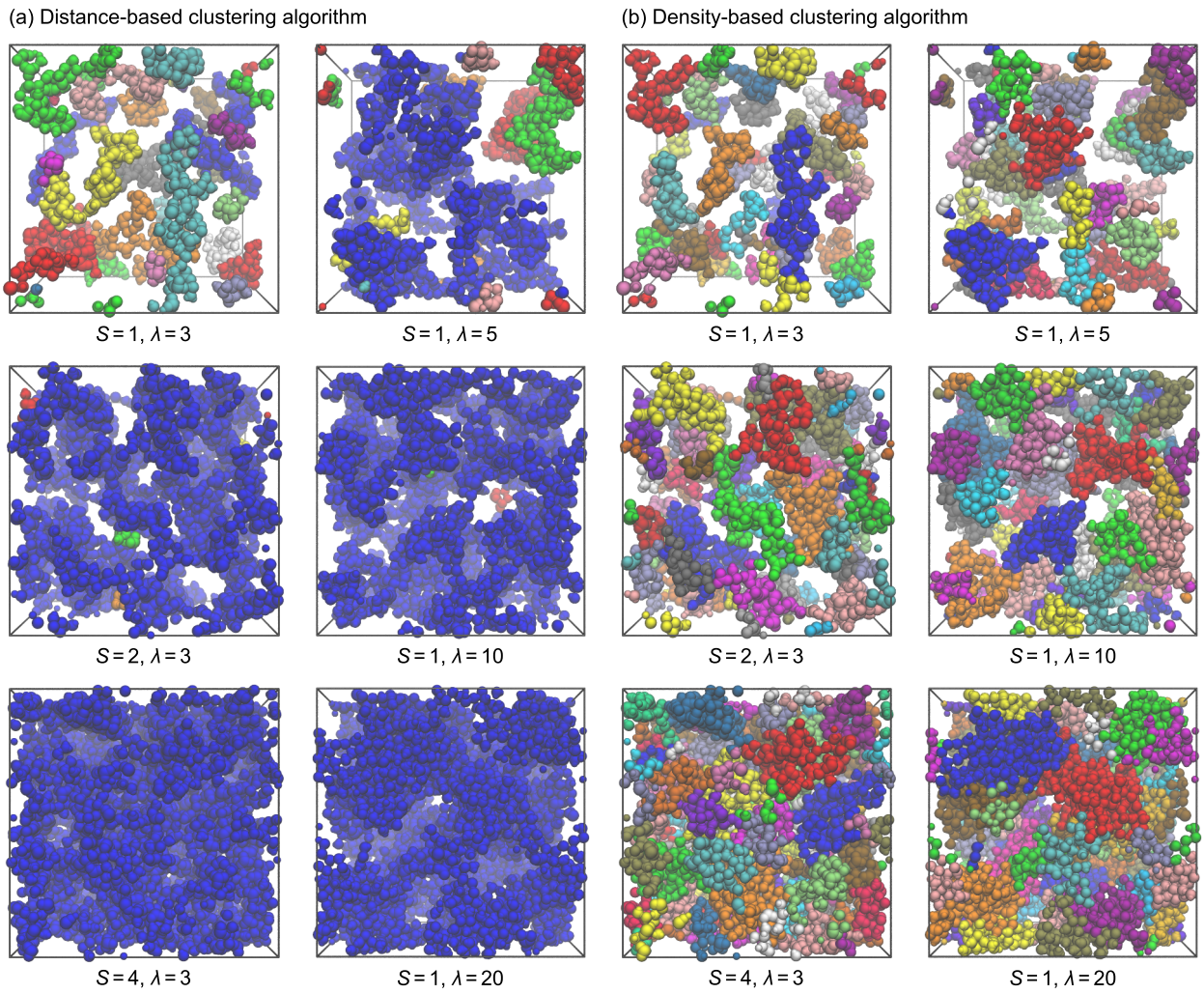

Figure 4: Snapshots of the hydrophilic domains in the simulations with each cluster given in a different color using the (a) distance-based algorithm and (b) density-based algorithm. The clustering analyses were performed on atoms in the sulfonate groups, hydronium ions, and water molecules only, as shown.

affects ionic aggregation in SDAPP. Specifically, atoms within the same sulfonate group, hydronium ion, or water molecule were assigned to the same cluster, and nearby groups were clustered together if any hydrogen bonding O–H or O–O pair was closer than a given cutoff distance. Specifically, cutoff distances were chosen to include the first peak in the corresponding RDFs. As illustrated in the snapshots in Figure 4a, we found that the ionic domains grew in size at larger sulfonation and hydration levels to form a large cluster spanning the periodic boundaries in the majority of the systems we studied. The cluster distributions are

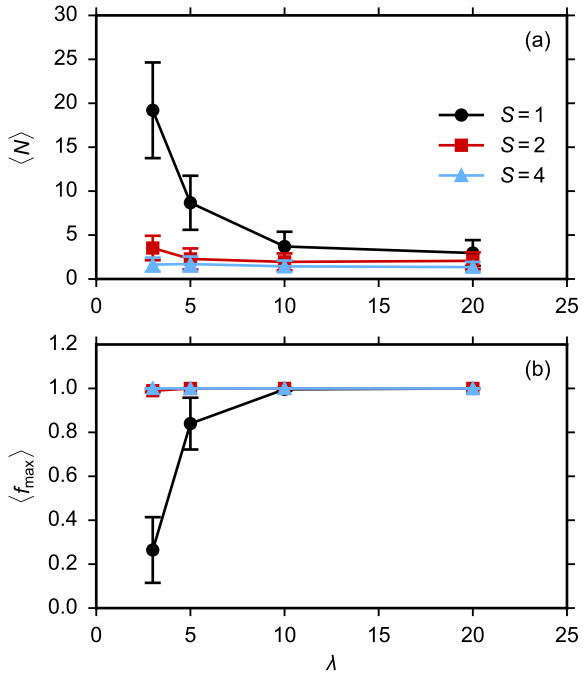

Figure 5: (a) The average number of clusters, $\langle N \rangle$, and (b) the average fraction of sulfonate groups in the largest cluster, $\langle f_{\max} \rangle$, as a function of hydration level, λ, for varying sulfonation levels. The points and error bars indicate the mean and standard deviation.

quantitatively compared in Figure 5, which plots the average number of clusters, $\langle N \rangle$, and the average fraction of sulfonate groups in the largest cluster, $\langle f_{\max} \rangle$. For a sulfonation level of $S = 1$, $\langle N \rangle$ decreased significantly from 19.2 to 3.0 with increasing water content. Additionally, $\langle f_{\max} \rangle$ increased from 26% to 100%. For sulfonation levels of $S = 2$ and 4, $\langle N \rangle < 4$ and $\langle f_{\max} \rangle \geq 99\%$ at all hydration levels. These results show that the simulations contained a large extended cluster containing nearly all ionic groups in all systems we studied, except at a sulfonation level of $S = 1$ with lower hydration levels of $\lambda = 3$ and 5.

Following the density-based clustering algorithm, we assigned two parameters to each atom: (i) ρ_i, which describes the local density as the number of atoms within a given cutoff distance, r_c, and (ii) δ_i, the minimum distance from an atom of higher density. Cluster centers were defined as atoms with $\delta_i > \delta_{\min}$, and all remaining atoms were assigned to the same cluster as its nearest neighbor of higher density. Here, we defined r_c and $\delta_{\min}$ to include the first peak in the SO–SO RDFs. The calculation of ρ_i was weighted by atomic masses and performed using a Gaussian kernel, which gave greater weight to atoms separated

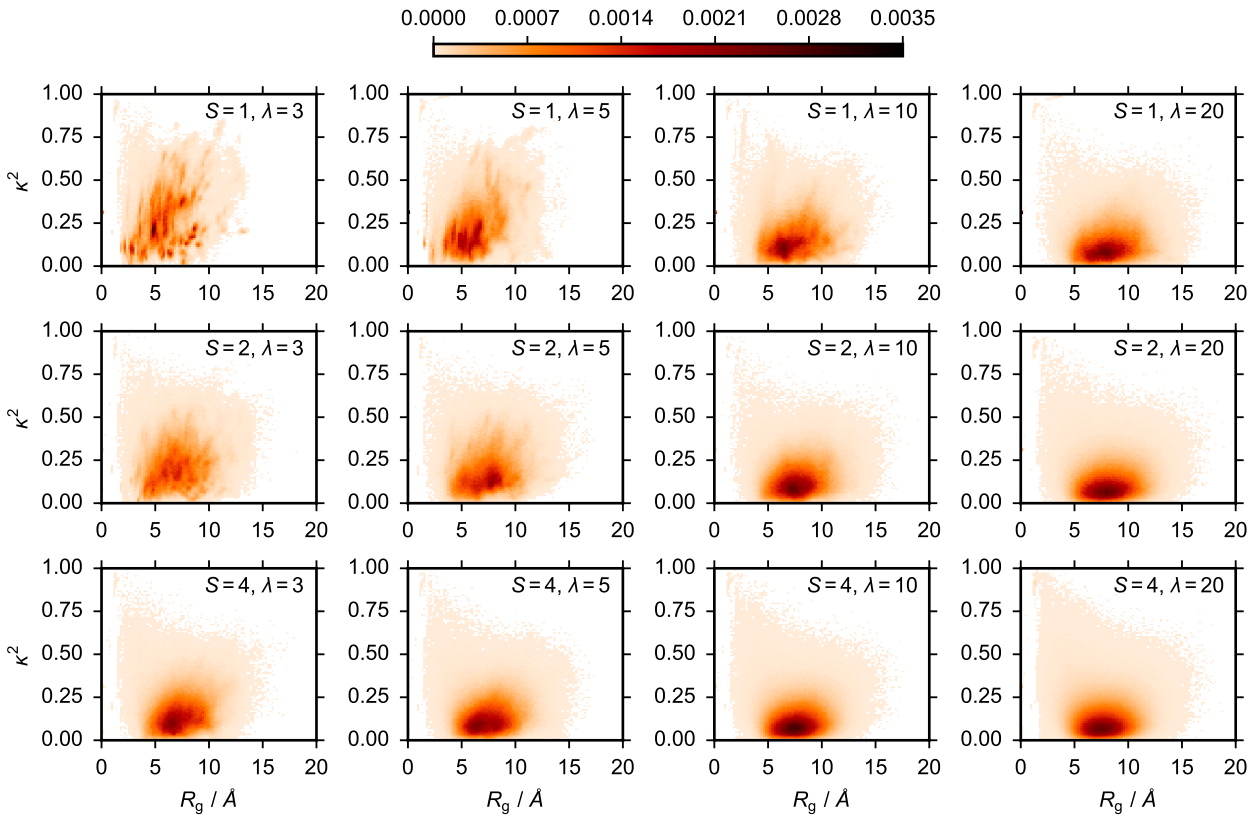

Figure 6: Two-dimensional histograms of the relative shape anisotropy, κ^2, versus the radius of gyration, R_g, of the clusters for each system varying the sulfonation level (top to bottom) and hydration level (left to right). All systems use the same color map given above the plots, with darker colors indicating regions populated more frequently during the simulations.

by smaller distances. The snapshots in Figure 4b show that this density-based algorithm yielded a more localized definition of clusters, where ionic aggregates connected by small water bridges were counted as distinct clusters. For each cluster, we described the size using the radius of gyration, $R_g^2 = \lambda_1 + \lambda_2 + \lambda_3$, where λ_1, λ_2, and λ_3 are the principal moments of the gyration tensor, and the shape using the relative shape anisotropy, $\kappa^2 = 1 - 3(\lambda_1\lambda_2 + \lambda_1\lambda_3 + \lambda_2\lambda_3)/R_g^4$, which spans from 0 for spherically symmetric shapes to 1 for a linear rod. In Figure 6, two-dimensional histograms of κ^2 versus R_g are shown for each system, where darker colors indicate regions populated more often during the simulations. At low sulfonation and hydration levels, R_g primarily ranged between 2 and 10 Å with a variety of cluster shapes between almost spherical with $\kappa^2 \approx 0$ to elongated and stringy with κ^2 up to 0.75. On the other hand, at larger sulfonation and hydration levels, clusters were

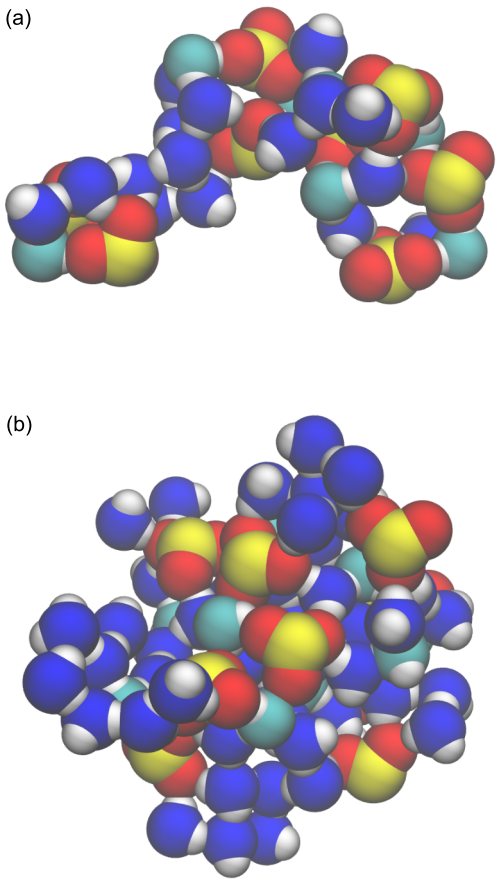

Figure 7: Examples of (a) an elongated cluster at a sulfonation level of $S = 1$ and hydration level of $\lambda = 3$, and (b) a spherical cluster at a sulfonation level of $S = 4$ and hydration level of $\lambda = 10$. Sulfur atoms are shown in yellow, sulfonate oxygens in red, water oxygens in blue, hydronium oxygens in cyan, and hydrogen atoms in white.

almost exclusively spherical in shape and slightly larger with R_g mainly between 5 and 10 Å. Two example clusters are compared in Figure 7 of an elongated cluster with $\kappa^2 = 0.40$ at a sulfonation level of $S = 1$ and hydration level of $\lambda = 3$, and a spherical cluster with $\kappa^2 = 0.05$ at a sulfonation level of $S = 4$ and hydration level of $\lambda = 10$.

Because R_g yields a single value over all three dimensions, it can be a misleading descriptor in non-spherical shapes (i.e., $\kappa^2 \gg 0$). For example, both clusters in Figure 7 have similar R_g values of 7.6 and 7.7 Å, respectively. As another quantitative measure of the size, we calculated the compositions of the clusters in terms of the median number of sulfurs, N_{SO}, hydronium oxygens, N_{OWH}, and water oxygens, N_{OW}, which are shown in Figure 8 for

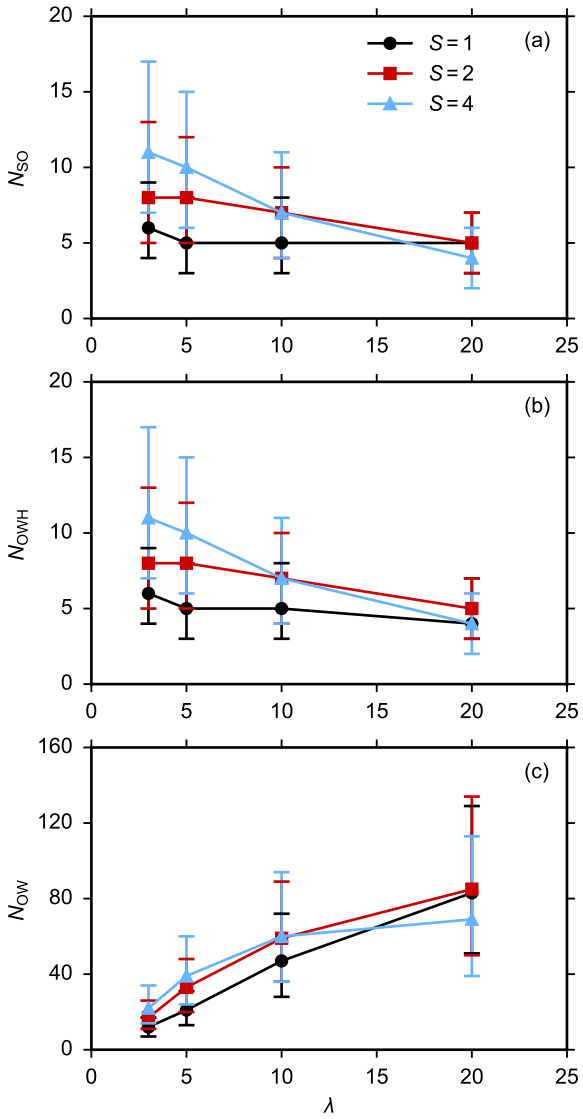

Figure 8: The average number of (a) sulfurs, N_{SO}, (b) hydronium oxygens, N_{OWH}, and (c) water oxygens, N_{OW}, per cluster as a function of hydration level, λ, for varying sulfonation levels. The points and error bars indicate the median and interquartile range.

all systems. At each sulfonation and hydration level, N_{SO} and N_{OWH} were very similar with values between 4 and 11, indicating that clusters tended to remain charge neutral. In particular, these values remained fairly constant at a sulfonation level of $S = 1$ and decreased only slightly with increasing water content at sulfonation levels of $S = 2$ and 4. On the other hand, N_{OW} increased significantly with water content at all degrees of sulfonation. For example, N_{OW} increased from 12 to 83 with increasing hydration at a sulfonation level of $S = 1$. Given that the number of ionic groups per cluster did not change significantly with

the sulfonation and hydration level, this suggests that the changes in size and shape resulted mainly from the addition of water molecules to the clusters. This is illustrated by the example clusters in Figure 7, which have a similar number of ionic groups, $N_{\mathrm{SO}} = N_{\mathrm{OWH}} = 8$ and 11, respectively, but a vastly different number of water molecules, $N_{\mathrm{OW}} = 16$ and 60, respectively.

Using complementary distance-based and density-based clustering algorithms, we have provided a thorough description of the nanoscale morphology of the ionic domains, including information about the size, shape, and connectivity of the ionic aggregates. From this improved understanding, we can also infer structural implications on ion transport. At the lowest sulfonation level of $S = 1$ and lower hydration levels of $\lambda = 3$ and 5, we found that clusters were formed in a variety of elongated and spherical shapes with a small number of water molecules bridging between the sulfonate groups. In particular, these were discrete ionic aggregates that did not percolate across the entire system. In these cases, ion transport would be hindered by small clusters and narrow water bridges, as well as slow structural rearrangements required to allow ions to hop between disparate clusters. At greater sulfonation levels of $S = 2$ and 4, fully percolated ionic domains were formed even at low water contents. In addition, larger spherical clusters were formed at the higher hydration levels through the addition of many water molecules to the ionic aggregates. Greater ion transport would be expected in these cases, as ions could move more freely within the solvated clusters and jump between connected neighboring clusters across larger water bridges. Improved ion transport with larger sulfonation levels is consistent with the experimental conductivity, which increases with increasing IEC.[9,10]

4 Conclusions

In this work, we presented atomistic simulations on a series of sulfonated polyphenylenes varying both the sulfonation and hydration levels. Given the hindered dynamics of these

glassy polymers, we designed an equilibration protocol with simulations at high temperatures and pressures to ensure that equilibrated systems were achieved at experimentally realistic densities. We then examined the local structure of the hydrophilic domains using radial distribution functions and coordination numbers, which yielded interesting insight into the strength of interactions between the ionic groups. In particular, sulfonate groups were surrounded by more water molecules and pushed further apart when the water content was increased, but retained similar spacings with increasing sulfonation. At low hydration, hydronium ions remained mostly in the first hydration shell of the sulfonate groups due to the strong electrostatic interactions. However, at higher hydration levels, more water molecules solvated the sulfonate groups and hydronium ions, such that the hydronium ions were to able to migrate out of the first solvation shell more often. Therefore, we would expect to see greater ion transport at larger degrees of sulfonation and water content, given the reduced strength of the ionic interactions and increased proportion of solvent-separated ion pairs.

At all sulfonation and hydration levels studied, we observed phase separation into nanoscale hydrophobic and hydrophilic domains, which was driven by the strong ionic interactions. We used two different clustering algorithms to obtain complementary insight into the nanoscale morphology of the hydrophilic domains formed by the ionic groups and water molecules. A distance-based algorithm provided information about the connectivity of the clusters. In particular, many distinct clusters were observed in systems with low degrees of sulfonation and water content, while a large, fully percolated cluster containing nearly all ionic groups was formed otherwise. Using a density-based algorithm, we achieved a more localized definition of the ionic aggregates to provide a quantitative comparison of the size and shape of the clusters. A broad range of cluster shapes were common at low degrees of sulfonation and water content, including elongated clusters with narrow water bridges between sulfonate groups. As the sulfonation and hydration levels were increased, clusters became more spherical in shape and grew slightly to incorporate a larger number of water molecules. The greater hydration, larger sizes, and extensive connectivity of the ionic domain would enable

improved ion transport at larger degrees of sulfonation and water content.

Due to limitations in experimental techniques, the nanoscale structure and morphology of SDAPP has remained somewhat elusive. To this end, the atomistic simulations we have presented in this work have provided a better understanding of the structure of the hydrophilic domains and insight into its possible effects on ion transport. Although our analysis has focused on the structural nature of SDAPP, we plan to investigate the dynamic properties of these systems more directly in future studies. Additionally, we hope to use these simulations to compare with and help interpret experimental results for a more complete understanding of the structure and properties of SDAPP.

Acknowledgement

The authors thank Cy Fujimoto, Todd Alam, Eric Sorte, Karen Winey, and Philip Griffin for useful discussions. This work was supported by the Laboratory Directed Research and Development program at Sandia National Laboratories, a multi-mission laboratory managed and operated by Sandia Corporation, a wholly owned subsidiary of Lockheed Martin Corporation, for the U.S. Department of Energy's National Nuclear Security Administration under contract DE-AC04-94AL85000.

References

(1) Wang, Y.; Chen, K. S.; Mishler, J.; Cho, S. C.; Adroher, X. C. A Review of Polymer Electrolyte Membrane Fuel Cells: Technology, Applications, and Needs on Fundamental Research. *Appl. Energy* **2011**, *88*, 981–1007.

(2) Merle, G.; Wessling, M.; Nijmeijer, K. Anion Exchange Membranes for Alkaline Fuel Cells: A Review. *J. Membr. Sci.* **2011**, *377*, 1–35.

(3) Li, N.; Guiver, M. D. Ion Transport by Nanochannels in Ion-Containing Aromatic Copolymers. *Macromolecules* **2014**, *47*, 2175–2198.

(4) Hickner, M. A.; Ghassemi, H.; Kim, Y. S.; Einsla, B. R.; McGrath, J. E. Alternative Polymer Systems for Proton Exchange Membranes (PEMs). *Chem. Rev.* **2004**, *104*, 4587–4612.

(5) Higashihara, T.; Matsumoto, K.; Ueda, M. Sulfonated Aromatic Hydrocarbon Polymers as Proton Exchange Membranes for Fuel Cells. *Polymer* **2009**, *50*, 5341–5357.

(6) de Araujo, C. C.; Kreuer, K. D.; Schuster, M.; Portale, G.; Mendil-Jakani, H.; Gebel, G.; Maier, J. Poly(p-phenylene sulfone)s with high ion exchange capacity: ionomers with unique microstructural and transport features. *Phys Chem Chem Phys* **2009**, *11*, 3305.

(7) Elabd, Y. A.; Hickner, M. A. Block Copolymers for Fuel Cells. *Macromolecules* **2011**, *44*, 1–11.

(8) Park, C. H.; Lee, C. H.; Guiver, M. D.; Lee, Y. M. Sulfonated Hydrocarbon Membranes for Medium-Temperature and Low-Humidity Proton Exchange Membrane Fuel Cells (PEMFCs). *Prog. Polym. Sci.* **2011**, *36*, 1443–1498.

(9) Fujimoto, C. H.; Hickner, M. A.; Cornelius, C. J.; Loy, D. A. Ionomeric Poly(phenylene) Prepared by Diels–Alder Polymerization: Synthesis and Physical Properties of a Novel Polyelectrolyte. *Macromolecules* **2005**, *38*, 5010–5016.

(10) Hickner, M. A.; Fujimoto, C. H.; Cornelius, C. J. Transport in Sulfonated Poly(phenylene)s: Proton Conductivity, Permeability, and the State of Water. *Polymer* **2006**, *47*, 4238–4244.

(11) Tang, Z.; Lawton, J. S.; Sun, C.-N.; Chen, J.; Bright, M. I.; Jones, A. M.; Papandrew, A. B.; Fujimoto, C. H.; Zawodzinski, T. A. Characterization of Sulfonated Diels-

Alder Poly (phenylene) Membranes for Electrolyte Separators in Vanadium Redox Flow Batteries. *J. Electrochem. Soc.* **2014**, *161*, A1860–A1868.

(12) Lawton, J. S.; Jones, A. M.; Tang, Z.; Lindsey, M.; Fujimoto, C.; Zawodzinski, T. A. Characterization of Vanadium Ion Uptake in Sulfonated Diels Alder Poly(phenylene) Membranes. *J. Electrochem. Soc.* **2016**, *163*, A5229–A5235.

(13) Hickner, M. A.; Pivovar, B. S. The Chemical and Structural Nature of Proton Exchange Membrane Fuel Cell Properties. *Fuel Cells* **2005**, *5*, 213–229.

(14) Hickner, M. A. Water-Mediated Transport in Ion-Containing Polymers. *J. Polym. Sci. Part B: Polym. Phys.* **2012**, *50*, 9–20.

(15) Cui, S.; Liu, J.; Selvan, M. E.; Keffer, D. J.; Edwards, B. J.; Steele, W. V. A Molecular Dynamics Study of a Nafion Polyelectrolyte Membrane and the Aqueous Phase Structure for Proton Transport. *J. Phys. Chem. B* **2007**, *111*, 2208–2218.

(16) Devanathan, R.; Venkatnathan, A.; Dupuis, M. Atomistic Simulation of Nafion Membrane: I. Effect of Hydration on Membrane Nanostructure. *J. Phys. Chem. B* **2007**, *111*, 8069–8079.

(17) Knox, C. K.; Voth, G. A. Probing Selected Morphological Models of Hydrated Nafion Using Large-Scale Molecular Dynamics Simulations. *J. Phys. Chem. B* **2010**, *114*, 3205–3218.

(18) Liu, J.; Suraweera, N.; Keffer, D. J.; Cui, S.; Paddison, S. J. On the Relationship Between Polymer Electrolyte Structure and Hydrated Morphology of Perfluorosulfonic Acid Membranes. *J. Phys. Chem. C* **2010**, *114*, 11279–11292.

(19) Daly, K. B.; Benziger, J. B.; Debenedetti, P. G.; Panagiotopoulos, A. Z. Molecular Dynamics Simulations of Water Sorption in a Perfluorosulfonic Acid Membrane. *J. Phys. Chem. B* **2013**, *117*, 12649–12660.

(20) Vishnyakov, A.; Neimark, A. V. Specifics of Solvation of Sulfonated Polyelectrolytes in Water, Dimethylmethylphosphonate, and Their Mixture: A Molecular Simulation Study. *J. Chem. Phys.* **2008**, *128*, 164902.

(21) Mahajan, C. V.; Ganesan, V. Influence of Hydrogen Bonding Effects on Methanol and Water Diffusivities in Acid–Base Polymer Blend Membranes of Sulfonated Poly(ether ether ketone) and Base Tethered Polysulfone. *J. Phys. Chem. B* **2013**, *117*, 5315–5329.

(22) Chang, Y.; Mohanty, A. D.; Smedley, S. B.; Abu-Hakmeh, K.; Lee, Y. H.; Morgan, J. E.; Hickner, M. A.; Jang, S. S.; Ryu, C. Y.; Bae, C. Effect of Superacidic Side Chain Structures on High Conductivity Aromatic Polymer Fuel Cell Membranes. *Macromolecules* **2015**, *48*, 7117–7126.

(23) Bahlakeh, G.; Hasani-Sadrabadi, M. M.; Jacob, K. I. Exploring the Hydrated Microstructure and Molecular Mobility in Blend Polyelectrolyte Membranes by Quantum Mechanics and Molecular Dynamics Simulations. *RSC Adv.* **2016**, *6*, 35517–35526.

(24) in 't Veld, P. J.; Rutledge, G. C. Temperature-Dependent Elasticity of a Semicrystalline Interphase Composed of Freely Rotating Chains. *Macromolecules* **2003**, *36*, 7358–7365.

(25) http://montecarlo.sourceforge.net.

(26) Skalski, T. J. G.; Britton, B.; Peckham, T. J.; Holdcroft, S. Structurally-Defined, Sulfo-Phenylated, Oligophenylenes and Polyphenylenes. *J. Am. Chem. Soc.* **2015**, *137*, 12223–12226.

(27) Karayiannis, N. C.; Mavrantzas, V. G.; Theodorou, D. N. Detailed Atomistic Simulation of the Segmental Dynamics and Barrier Properties of Amorphous Poly(ethylene terephthalate) and Poly(ethylene isophthalate). *Macromolecules* **2004**, *37*, 2978–2995.

(28) Abbott, L. J.; Hart, K. E.; Colina, C. M. Polymatic: A Generalized Simulated Polymerization Algorithm for Amorphous Polymers. *Theor. Chem. Acc.* **2013**, *132*, 1334.

(29) Jorgensen, W. L.; Maxwell, D. S.; Tirado-Rives, J. Development and Testing of the OPLS All-Atom Force Field on Conformational Energetics and Properties of Organic Liquids. *J. Am. Chem. Soc.* **1996**, *118*, 11225–11236.

(30) Canongia Lopes, J. N.; Pádua, A. A. H.; Shimizu, K. Molecular Force Field for Ionic Liquids IV: Trialkylimidazolium and Alkoxycarbonyl-Imidazolium Cations; Alkylsulfonate and Alkylsulfate Anions. *J. Phys. Chem. B* **2008**, *112*, 5039–5046.

(31) Carrillo, J.-M. Y.; Dobrynin, A. V. Detailed Molecular Dynamics Simulations of a Model NaPSS in Water. *J. Phys. Chem. B* **2010**, *114*, 9391–9399.

(32) Dahlgren, M. K.; Schyman, P.; Tirado-Rives, J.; Jorgensen, W. L. Characterization of Biaryl Torsional Energetics and its Treatment in OPLS All-Atom Force Fields. *J. Chem. Inf. Model.* **2013**, *53*, 1191–1199.

(33) Jang, S. S.; Lin, S.-T.; Maiti, P. K.; Blanco, M.; Goddard III, W. A.; Shuler, P.; Tang, Y. Molecular Dynamics Study of a Surfactant-Mediated Decane-Water Interface: Effect of Molecular Architecture of Alkyl Benzene Sulfonate. *J. Phys. Chem. B* **2004**, *108*, 12130–12140.

(34) Abascal, J. L. F.; Vega, C. A General Purpose Model for the Condensed Phases of Water: TIP4P/2005. *J. Chem. Phys.* **2005**, *123*, 234505.

(35) Urata, S.; Irisawa, J.; Takada, A.; Shinoda, W.; Tsuzuki, S.; Mikami, M. Molecular Dynamics Simulation of Swollen Membrane of Perfluorinated Ionomer. *J. Phys. Chem. B* **2005**, *109*, 4269–4278.

(36) Plimpton, S. Fast Parallel Algorithms for Short-Range Molecular Dynamics. *J. Comput. Phys.* **1995**, *117*, 1–19.

(37) http://lammps.sandia.gov.

(38) Ryckaert, J.-P.; Ciccotti, G.; Berendsen, H. J. C. Numerical Integration of the Cartesian Equations of Motion of a System with Constraints: Molecular Dynamics of n-Alkanes. *J. Comput. Phys.* **1977**, *23*, 327–341.

(39) Humphrey, W.; Dalke, A.; Schulten, K. VMD: Visual Molecular Dynamics. *J. Mol. Graphics* **1996**, *14*, 33–38.

(40) Elliott, J. A.; Paddison, S. J. Modelling of Morphology and Proton Transport in PFSA Membranes. *Phys. Chem. Chem. Phys.* **2007**, *9*, 2602–2618.

(41) Clark II, J. K.; Paddison, S. J.; Eikerling, M.; Dupuis, M.; Zawodzinski Jr., T. A. A Comparative Ab Initio Study of the Primary Hydration and Proton Dissociation of Various Imide and Sulfonic Acid Ionomers. *J. Phys. Chem. A* **2012**, *116*, 1801–1813.

(42) Hall, L. M.; Seitz, M. E.; Winey, K. I.; Opper, K. L.; Wagener, K. B.; Stevens, M. J.; Frischknecht, A. L. Ionic Aggregate Structure in Ionomer Melts: Effect of Molecular Architecture on Aggregates and the Ionomer Peak. *J. Am. Chem. Soc.* **2012**, *134*, 574–587.

(43) Lin, K.-J.; Maranas, J. K. Cation Coordination and Motion in a Poly(ethylene oxide)-Based Single Ion Conductor. *Macromolecules* **2012**, *45*, 6230–6240.

(44) Bolintineanu, D. S.; Stevens, M. J.; Frischknecht, A. L. Influence of Cation Type on Ionic Aggregates in Precise Ionomers. *Macromolecules* **2013**, *46*, 5381–5392.

(45) Rodriguez, A.; Laio, A. Clustering by Fast Search and Find of Density Peaks. *Science* **2014**, *344*, 1492–1496.